JOINT INSTITUTE FOR NUCLEAR RESEARCH
Veksler and Baldin laboratory of High Energy Physics

FINAL REPORT ON THE START PROGRAMME

Simulating strange particles production near the threshold in pp, p-Au and Au-Au collisions

Supervisor:
Dr. Alexey Aparin

Student:
Oris Suárez Eng,
Instituto Superior de Tecnologías y Ciencias Aplicadas (InSTEC)

Participation period:
April 6th – June 2nd,
Winter Session 2024

Dubna, 2024

Acknowledgments

I would like to express my honest gratitude to my supervisor Dr. Alexey Aparin for given me the opportunity to visit JINR and work in his team. I felt welcomed from the very beginning of my stay.

And I cannot express in words how grateful I am of having met so many friendly, kind and helpful people during these two months. Your support and company made my Dubna journey one of the best professional and social experiences of my life. Thanks a lot to all of you.

Abstract

The study and understanding of the bulk properties of low centre-mass energy collisions is the general objective of NICA Complex. To this end, in this work, we examine the performance of the PYTHIA8.310 event generator and its newly implemented Angantyr model, to describe hadronic and heavy-ion collisions at low energy scales. We simulated five million pp and p-Au collision events per system, and one million Au-Au collision events at $\sqrt{s_{NN}}=5\,\mathrm{GeV}$. The pp and p-Au collision were considered in fixed-target mode and the Au-Au collision in collider mode. We report on the transverse momentum vs longitudinal momentum (p_T vs p_L), transverse momentum vs pseudorapidity (p_T vs η), rapidity and azimuthal angle distribution analysis for all final particles and for strange particles individually. In this manner, we study the lambda (Λ^0), sigma (Σ^+, Σ^0, Σ^-) and kaon (K^0, K^+, K^{*0}, K^{*+}) particles production.

Table of Contents

Introduction

The Quark-Gluon Plasma (QGP) is the deconfined state of strongly interacting matter. At low density and temperature, quarks are confined within the hadrons. Increasing the temperature of the system will result in low mass resonance production. A large number of resonances will make the system dense and hadrons can start interprenetrate each other resulting in a deconfined state of quarks and gluons. It can be seen as a confinement-deconfinement phase transition. Theoretical predictions indicate that beyond a critical energy density $\varepsilon_{cr} \sim 1\,\mathrm{GeV\,fm^{-3}}$, or temperature $T_{cr} \sim 200\,\mathrm{MeV}$, matter can only exist as QGP.

Fig 1. shows the phase diagram of the Quantum Chromodynamics (QCD) theory. It presents the phase transitions from nuclear matter to QGP state. Phase transitions are the thermodynamics singularities in a region formed by strongly interacting matter in thermal and chemical equilibrium. Accordingly, the phase diagram is described in terms of temperature (T) and net baryon density (n/n_o).

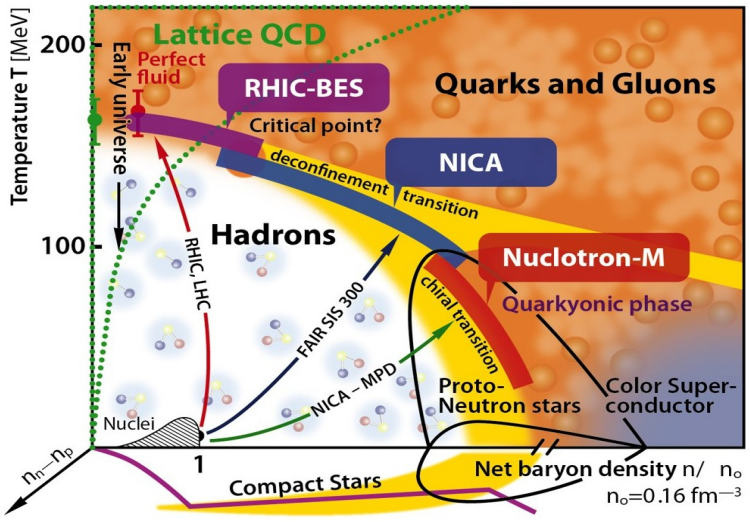

Figure 1: QCD phase diagram in Temperature (T) vs net baryon density (n/n_o) plane.

The region for low values of T and $n/n_o \sim 1$ corresponds to nuclear matter (protons and neutrons), and when the net baryon density is increased we reach atomic nuclei and neutron stars matter conditions. In contrast, for small values of n/n_o, by increasing the temperature, the system evolves to a hadron gas, but around the Hagedorn temperature $T_H \sim 170\,\mathrm{MeV}$ there is a crossover to the QGP state. Between these confined and deconfined phases there is a first order transition boundary that ends at the "critical point". This is a second-order phase transition point that leads towards the crossover region, and on top of it lies the quark-gluon plasma phase and below it the hadronic phase.

It is not yet known whether QCD has an actual critical point, nor where in its phase diagram it might lie. Hence, the search for the QCD critical point and overall study of the QCD phase transitions are an active area of research in the field of fundamental physics.

Large experimental facilities such as the Large Hadron Collider (LHC) and the Relativistic Heavy Ion Collider (RHIC), with the work of nearly three decades, have successfully recreate QGP conditions at the laboratory and proposed several conserved quantities in strong interactions that could be sensitive to the physics of the critical point. However, the results obtained so far concerned only regions with high temperature and baryon density close to zero or below it, when the ratio of baryons and anti-baryons are almost identical. Nevertheless, the properties of matter at lower temperature and higher baryon density values remain open to study and exploration. This represents the general physics goal of the STAR experiment at RHIC and the forthcoming MPD experiment at NICA.

STAR Experiment

The Solenoidal Tracker at RHIC (STAR) is one of the two large detector systems constructed at the Relativistic Heavy Ion Collider at Brookhaven National Laboratory [1]. It was initially built for ultra-relativistic heavy ion collisions. Nowadays, it also includes proton-proton and proton-nucleus interactions to understand the initial PDF of the incident nuclei and as a baseline for heavy ion collision studies [12].

Mapping the QCD phase structure at high baryon density, namely the first-order phase transition boundary and the location of the critical point, is the primary goal of the Beam Energy Scan (BES) program at RHIC. The STAR experiment has been studying Au-Au collision at $\sqrt{s_{NN}} = 7.7 - 200\,\text{GeV}$ in collider mode. However, in 2015 the STAR Fixed-Target (FXT) program was conducted to achieve lower centre-mass energies, which allows the access to the QCD phase diagram region with μ_B up to 750 MeV [14]. Recently, new phenomena in the production dynamics of light nuclei [16] and strangeness production [15] at such energy scales are been reported.

NICA Complex

NICA (**N**uclotron-based **I**on **C**ollider f**A**cility) is a new accelerator complex design at the Joint Institute for Nuclear Research (JINR) in Dubna, Russia. The purpose of the mega-science project "NICA Complex" is to conduct fundamental research on the most relevant issues of modern particle physics [2]. Its experimental facilities are shown in fig 2.

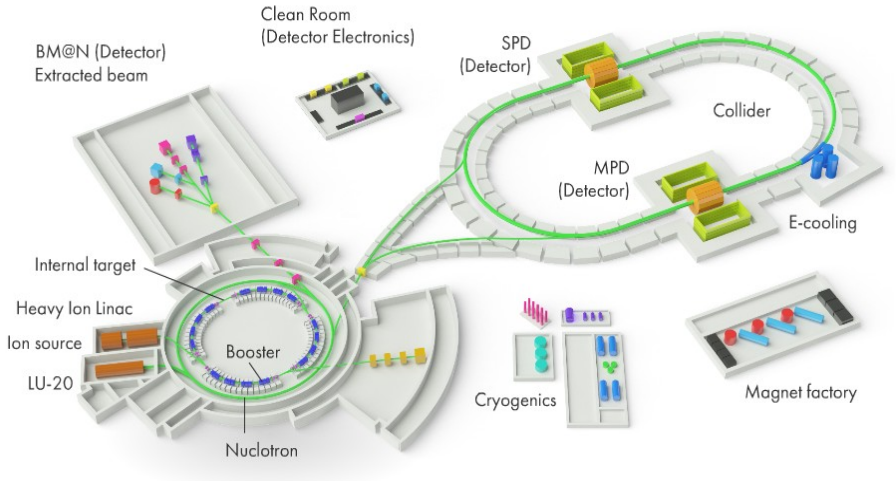

Figure 2: Layout of the main accelerators and experimental facilities at NICA Complex [3]

The heart of NICA Complex is the Nuclotron accelerator, which is operating since 1993. The ion beams are provided by two injection complexes. The KRION-6T (Ion source) coupled to the HiLac (Heavy Ion Linac) produce light ions up to carbon. Dedicated sources with LU-20 linac produce heavier ions, including krypton, xenon and bismuth. Both sources are commissioned and operating. The Nuclotron is a circular accelerator based on fast-cycling superconducting magnets, able to accelerate ions from protons up to bismuth with maximum kinetic energy of 3.8 GeV/u for Au ions. Booster is an auxiliary accelerator for pre-acceleration of heavy ions up to 600 MeV/u. Both Booster and Nuclotron will provide beams of ions to the Baryonic Matter at Nuclotron (BM@N) [7], the Spin Physics Detector (SPD) [6] and the Multi-Purpose Detector (MPD) [8] experiments.

NICA is a racetrack-shaped collider, with 503 m of circumference. NICA is designed to provide Au+Au collisions in the centre-mass energy $\sqrt{s_{NN}}$ range of 4 to 11 GeV. It can accelerate ions from protons and deuterons, intermediate (Ar, Fe, Kr, Xe and others) up to heavy ions (Au, Bi) [4].

The main directions of the research program at NICA Complex are:

- Search and experimental study of phase transitions and critical phenomena in strongly interacting nuclear matter at extreme baryonic densities.
- Experimental study of the spin structure of nucleon and light nuclei
- Investigation of polarization effects in heavy ion collisions and few nucleon systems.
- Investigation of reaction dynamics and studying modifications of hadron properties in nuclear matter.

- Study of the structure of the nuclei at short internucleon distances, near-treshold strange hyperon production and search for hypernuclei of the Nuclotron extracted ion beams with fixed targets.
- Development of theoretical models of the studied processes and theoretical support of experiments.

Theoretical studies at NICA combine a detailed simulation process of experiments with specific conditions to explore new theoretical methods, in particular, non-perturbative and lattice quantum chromodynamics. Further information on the research program and experimental details can be found in [2] and [5].

Multi-Purpose Detector

The Multi-Purpose Detector (MPD) is one of the two dedicated heavy-ion collision experiments of NICA Complex. Its main scientific purpose is to search for novel phenomena in the baryon-rich region of the QCD phase diagram by means of colliding heavy nuclei in the centre-mass energy $4 < \sqrt{s_{NN}} < 11$ GeV. The NICA-MPD experimental program will fill a niche in the energy scale, which is not yet fully explored, and the results will bring about a deeper insight into hadron dynamics and multiparticle production in the high baryon density domain. Its is foreseen that the MPD apparatus will be installed in two stages. The first stage of the detector configuration is planned to be ready for commissioning in 2025. The overall setup and the spatial arrangement of the detector subsystems on the first stage are shown in Fig 3.

The "central barrel" components have an approximate cylindrical symmetry within $|\eta|<1.5$. The beam line is surrounded by the large volume Time Projection Chamber (TPC) which is enclosed by the TOF barrel. TPC is the main tracker, and together with TOF they will provide precise measurements and particle identification. ECal is the Electromagnetic Calorimeter, placed in between TOF and the MPD magnet. It will be used for detection of electromagnetic showers, and will play the central role in photon and electron measurements. The MPD superconducting solenoid magnet is designed to provide a highly homogeneous magnetic field of up to 0.57 T, uniform along the beam axis, to ensure appropriate transverse momentum resolution for reconstructed particles within the range of momenta of 0.1-3 GeV/c. As the average transverse momentum of the particles produced in a collision at NICA energies is below 500 MeV/c, the detector was designed to have a very low material budget. The Forward Hadronic Calorimeter (FHCal) is located near the magnet end-caps. It will serve for determination of the collision centrality and the orientation of the reaction plane for collective flow studies [8]. The silicon-based Inner Tracking System (ITS) will be installed close to the interaction point in the second stage

of the MPD construction. It will greatly enhance tracking and secondary vertex reconstruction capabilities.

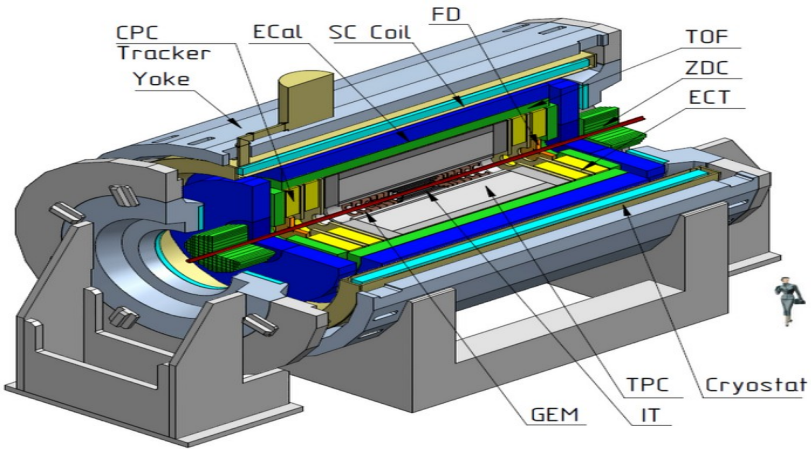

Figure 3: A general view of the MPD detector.

In order to study the QCD phase diagram at high baryon densities values, and temperature, the MPD main areas of research will be [2]:

- yield of strange particles, baryons and anti-baryons,
- event-by-event fluctuation of multiparticle production, transverse momentum, ratios of particle yields,
- anisotropic and collective flows,
- pulse correlations (femtoscopy),
- production of lepton pairs and soft photons,
- polarization phenomena.

Project goals

Since the MPD/NICA Complex program is under development, it is necessary to have assistance from simulation frameworks that could provide confirmation and predictions of theoretical models and experimental setups, prior to the first collider runs. The center-mass energy range of $4 < \sqrt{s_{NN}} < 11$ GeV encounters several challenges when finding a suitable theoretical model to describe observations. At such energy scales, resonance production, nuclear structure effects, cluster formation and isospin effects are unique

phenomena that are not observed, nor dominant, in high energy collisions. Moreover, there is often less experimental data available for benchmarking and validating the models.

Multiple models for low energy scales have been implemented in heavy-ion collision event generators as EPOS [9], UrQMD [10], PHSD, SMASH [11]. Some of these models provide detailed description for initial state fluctuations, including partonic interactions, as it is the case for EPOS and PHSD; others present more comprehensible representation of hadronic interactions and resonance decays (UrQMD). Still, the search for a general-purpose heavy-ion collision model, specially for low energy scales, is still a goal in modern physics.

PYTHIA8 is a general-purpose event generator for the simulation of hadronic and leptonic interactions mostly at high energy scales (those managed at LHC). Relatively recently, the Pythia8 event generator implemented a heavy-ion collision model. Angantyr is a new model for high-energy pA and AA collisions that, in comparison with other models, it accounts for fluctuations in both projectile and target nucleons. It is an extrapolation from pp interaction with a minimum of free parameters, inspired by the Fritiof model [13]. In terms os studying the collectivity of final charged particles produced in nuclei collisions, the Angantyr model does not make any attempt to model such effects. However, the probes in the model show that it gives a good description of general final state properties, including multiplicity, transverse momentum and its dependence of centrality.

For this project, we want to examine the Pythia8 and the Angantyr model performance describing the bulk properties and strange particles production of hadronic and heavy-ions collision systems at low energy scales. Analysis on the p_T vs p_L, p_T vs η, particle production and azimuthal angle (φ) and pseudorapidity (η) distribution will be conducted.

Scope of work

We aim to contribute to the study of the bulk properties of pp, p-Au and Au-Au collision systems for the forthcoming MPD/NICA experiment, using the Pythia8 event generator.

Methods

Perform the simulations of the pp, p-Au and Au-Au collisions with the Pythia8 event generator. Find the proper setting parameters to describe these hadronic and heavy-ion collision systems at $\sqrt{s_{NN}}=5\,\mathrm{GeV}$. Study the lambda ($\Lambda^0$), sigma ($\Sigma^+$, Σ^0, Σ^-) and kaon (K^0, K^+, K^{*0}, K^{*+}) particles to analyze strange particle production.

Results

We present the p_T vs p_L, p_T vs η, rapidity (y) and azimuthal angle (φ) distribution analysis in pp, p-Au and Au-Au collisions at $\sqrt{s_{NN}}=5\,\text{GeV}$ centre-mass energy for all final particles and for lambda (Λ^0), sigma (Σ^+, Σ^0, Σ^-) and kaon (K^0, K^+, K^{*0}, K^{*+}) particles specifically. The PYTHIA8.3 event generator and the Angantyr model were used for the simulation of the aforementioned colliding system, in which 5×10^6 events were analyzed for the pp and p-Au systems and 1×10^6 events for the Au-Au system.

The fixed-target collision type in Pythia can be turn on with the settings "Beams:frameType = 2", and specifying the energies for each beam. For pp collision, one of the protons is at rest ($\vec{p}=0$) and the other moves with $\vec{p}=12\,\text{GeV}$. In the p-Au collision, the gold target is the stationary target. However, in the Au-Au collision no fixed-target experiment is considered. A colliding-beam system simulation is performed instead. We also included the "SoftQCD:all = on" setting to turn on all low energy QCD processes that could initiate the collision.

For the simulation of pp and pp^- collisions in Pythia8, the ABMST model includes sophisticated Pomeron-inspired framework, addressing total, elastic and single diffractive cross sections. The tuning to single diffractive data has mainly been performed at lower energies which makes it compelling to test in the NICA energy scales range. The ABMST model is included with the "SigmaTotal: mode = 3" and "SigmaDiffractive:mode = 3" master switches. And the Angantyr model for p-Au and Au-Au collisions is set automatically.

Transverse Momentum vs Longitudinal Momentum distribution

Fig 4 presents the transverse momentum (p_T) vs longitudinal momentum (p_L, in the z axis direction) distribution for the (a) pp, (b) p-Au and (c) Au-Au systems at $\sqrt{s_{NN}}=5\,\text{GeV}$. In the pp and p-Au collision we do not observe the p_L symmetry around $p_L = 0$ which is present in the Au-Au distribution. This is the result of considering a fixed-target experiment, where most of the particle scatter off in the beam direction (positive z axis). The Au-Au simulation is a colliding-beam system, particles scatter off in all directions around the interaction point.

Between the pp and p-Au collision there is also a shape difference in the distribution, which is the result of the asymmetry present in the p-Au collision.

The high-p_T particle production increases as the number of participant nucleons in the colliding systems does it. In pp, almost all particles present $p_T < 2.5$ GeV. However, the p-

Au system presents particles with higher transverse momentum which is then overcome in the Au-Au collision. This could be the result of jet quenching and energy loss mechanisms.

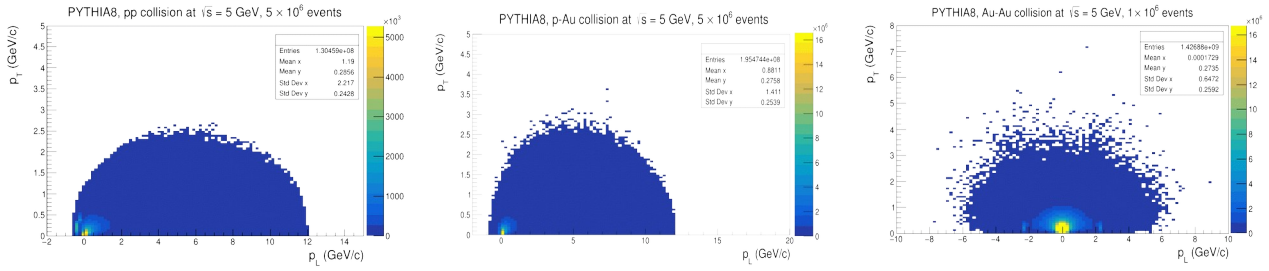

(a) (b) (c)

Fig 4: p_T vs p_L distribution in (a) pp, (b) p-Au, (c) Au-Au collision at $\sqrt{s_{NN}}$=5GeV with the PYTHIA8.3 event generator.

Analysis for lambda, sigma and kaon particles.

We perform the former analysis for lambda (Λ^0), sigma (Σ^+, Σ^0, Σ^-) and kaon (K^0, K^+, K^{*0}, K^{*+}) individually to analyze resonance production in these colliding systems.

In the Pythia8 event generator, lambda and sigma resonances decay into more stable hadrons and cannot be detected directly in the final state of the collision. To make them stable particles, detectable in the final state, we included the following settings: "3222:mayDecay = false", "3112:mayDecay = false", "3212:mayDecay = false" and "3122:mayDecay = false".

p_T vs p_L distribution analysis for lambda particles

Fig 5 present the p_T vs p_L distribution for the lambda particle in the a) pp, b) p-Au and c) Au-Au collision. The particle multiplicity increases with the colliding system. In pp there are 4000 events of lambda production, whilst in p-Au there are 6000 and in Au-Au 80000 events.

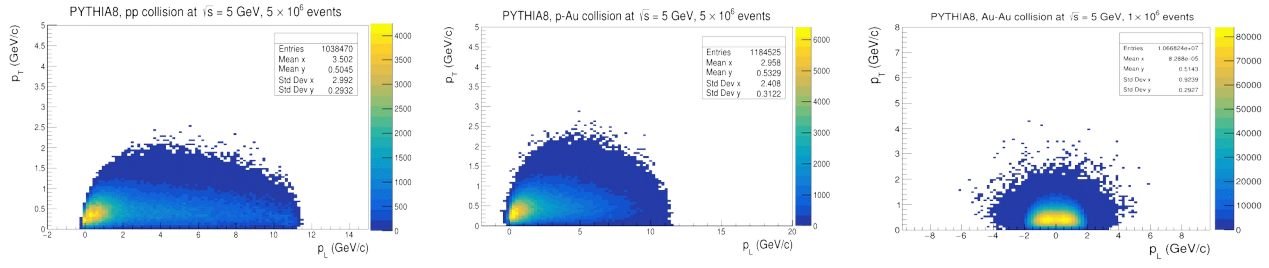

(a) (b) (c)

Fig 5: p_T vs p_L distribution for lambda particles (Λ^0) in (a) pp, (b) p-Au, (c) Au-Au collision at $\sqrt{s_{NN}}$=5GeV with the PYTHIA8.3 event generator.

The lambda production in all three systems also shows a certain transverse momentum limit around $1.2 < p_T < 1.4$ GeV, for the majority of events. Additionally, we observe the presence of a tail in the pp and p-Au systems. However, it present higher values of p_L in the pp system, up to 11 GeV, in contrast with p-Au.

p_T vs p_L distribution analysis for sigma particles

Fig 6 presents the p_T vs p_L distribution for sigma particles in the a) pp, b) p-Au and c)Au-Au collision. The particle multiplicity is less when compare with the lambda particle. The sigma particle production is less frequent than the lambda particle production. 1200 events show the presence of Σ^+, Σ^0 or Σ^- in pp, 4500 in p-Au and 60000 events in Au-Au.

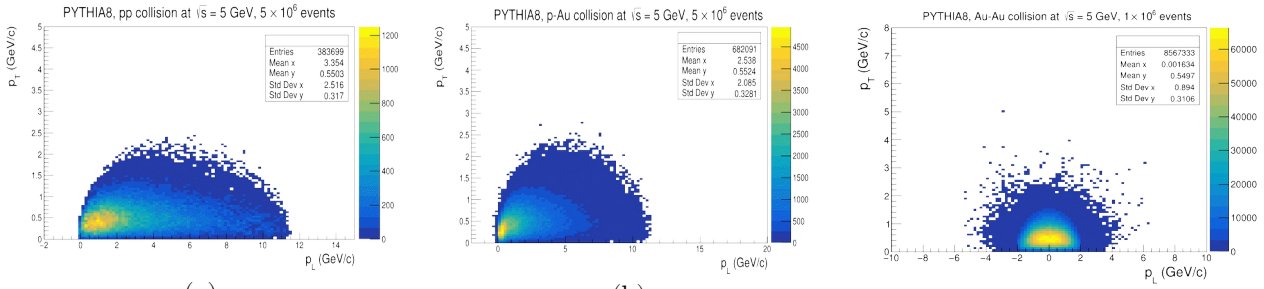

(a) (b) (c)

Fig 6: p_T vs p_L distribution for sigma particles (Σ^+, Σ^0, Σ^-) in (a) pp, (b) p-Au, (c) Au-Au collisions at $\sqrt{s_{NN}}$=5GeV with the PYTHIA8.3 event generator.

In the pp collision, the sigma particles where produced with larger values of p_L, with intense activity for p_L values up to 3 GeV, in contrast with the p-Au and Au-Au systems where the maximum activity concerns particles with p_L values up to 1.5 GeV.

p_T vs p_L distribution analysis for kaon particles

The p_T vs p_L analysis distribution for kaon particles (K^0, K^+, K^{*0}, K^{*+}) in a) pp, b) p-Au and c)Au-Au collisions is presented in Fig 7. The kaon multiplicity show similar features than that observed for the lambda and sigma particles.

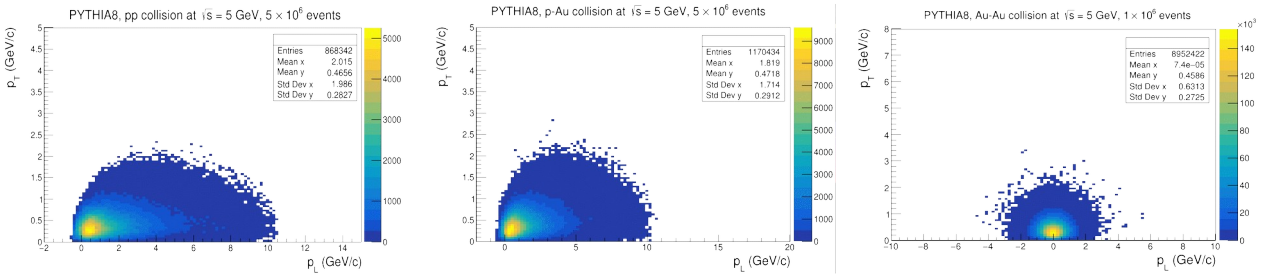

(a) (b) (c)

Fig 7: p_T vs p_L distribution for kaon particles (K^0, K^+, K^{*0}, K^{*+}) in (a) pp, (b) p-A, (c) Au-Au collisions at $\sqrt{s_{NN}}$=5 GeV with the PYTHIA8.3 event generator.

Transverse momentum vs pseudorapidity distribution

Fig 8 presents the transverse momentum (p_T) vs pseudorapidity (η) distribution for all final particles in a) pp, b) p-Au and c) Au-Au collisions.

In the pp and p-Au systems, we observe that the pseudorapidity distribution is asymmetrical with respect to the origin, which is not the case for the Au-Au collision. This is due to the fixed-target experiment consideration.

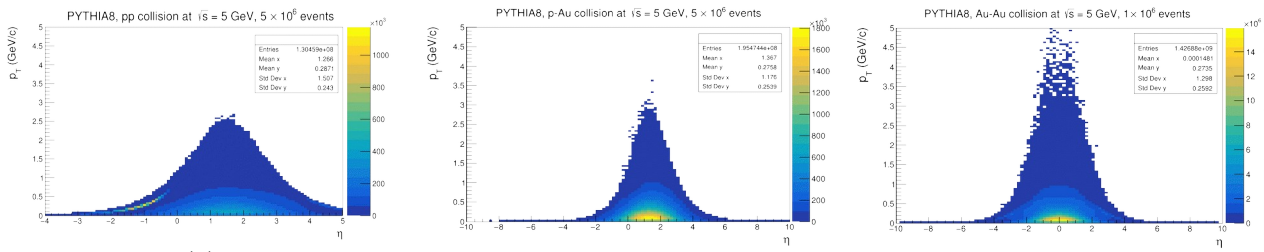

(a) (b) (c)

Fig 8: p_T vs η distribution in (a) pp, (b) p-Au, (c) Au-Au collision at $\sqrt{s_{NN}}$=5 GeV with the PYTHIA8.3 event generator.

Analysis for lambda, sigma and kaon particles.

We also perform the former analysis for lambda (Λ^0), sigma (Σ^+, Σ^0, Σ^-) and kaon (K^0, K^+, K^{*0}, K^{*+}) individually to study the angular distribution in the forward and backward directions with respect to the interaction point.

p_T vs η distribution for lambda particles

In Fig 9 we present the former the p_T vs η distribution for lambda particles in a) pp, b) p-Au and c) Au-Au collisions at $\sqrt{s_{NN}}$=5GeV. The maximum pseudorapidity value is around $\eta_{max} \cong 5$ for the pp, $\eta_{max} \cong 4$ for the p-Au and $\eta_{max} \cong 3$ for the Au-Au. And they have a maximum p_T for all three colliding systems of $p_T \cong 1.5$ GeV.

The symmetrical shape due to the symmetrical collision is observed in the Au-Au system.

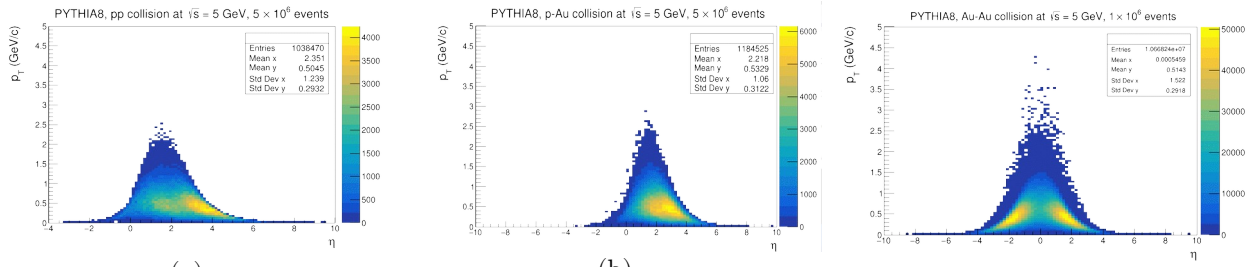

(a) (b) (c)

Fig 9: pT vs η for lambda particles (Λ^0) in (a) pp, (b) p-Au, (c) Au-Au collision at $\sqrt{s_{NN}}$=5GeV with the PYTHIA8.3 event generator.

p_T vs η distribution for sigma particles

The p_T vs η distribution for sigma particles in a) pp, b) p-Au and c) Au-Au collisions is presented in Fig 10.

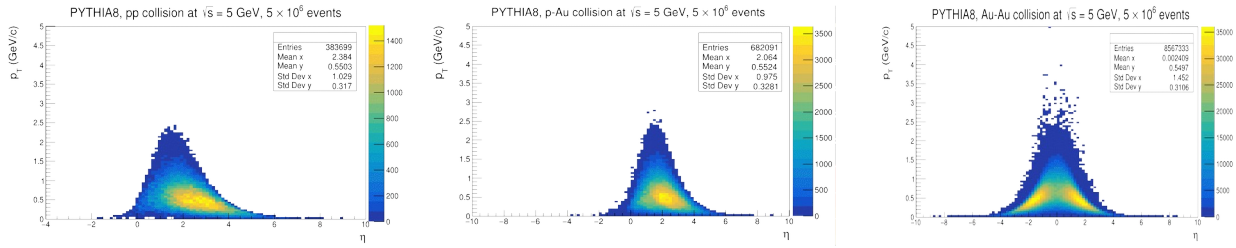

(a) (b) (c)

Fig 10: pT vs η for sigma particles in (a) pp, (b) p-Au, (c) Au-Au collision at $\sqrt{s_{NN}}$=5GeV

In the Au-Au collision, we observe that the most intensive region of the distribution is divided in two regions, symmetrical with respect to the origen. However, the intensity fades for small values of the pseudorapidity (- 0.2 < η < 0.2). Most of the particles are in either the forward or backward region of the interaction point. Few are located in the mid-

rapidity region. This is also observed in the p_T vs η distribution in Au-Au collision for lambda particles.

p_T vs η distribution for kaon particles

Fig 11 shows the p_T vs η analysis for kaon particles in a) pp, b) p-Au and c) Au-Au collisions.

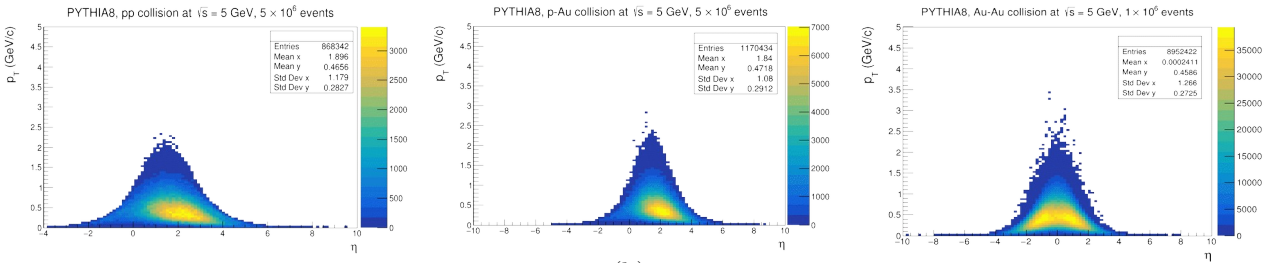

(a) (b) (c)

Fig 11: pT vs η for kaon particles in (a) pp, (b) p-Au, (c) Au-Au collision at $\sqrt{s_{NN}}$=5GeV

For the kaon particles, the observations in the Au-Au collision for lambda and sigma particles are not present. Here, kaon particles can be found in the forward, backward and mid-rapidity regions, which is not the case for lambda and sigma particles.

Rapidity distribution

We also analyzed the rapidity distribution for all final particles and for lamba, sigma and kaon particles individually in all three colliding system (pp, p-Au and Au-Au) at a centre-mass energy of $\sqrt{s_{NN}}$=5GeV.

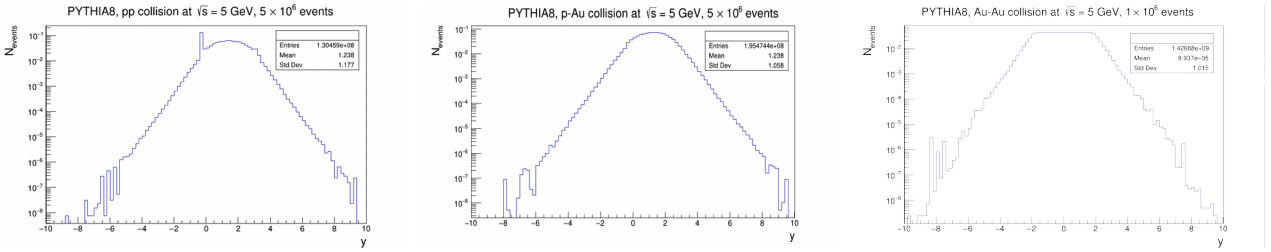

(a) (b) (c)

Fig 12: Rapidity distribution for final particles in (a) pp, (b) p-Au and (c) Au-Au collision at $\sqrt{s_{NN}}$=5GeV

Fig 12 presents the overall rapidity distribution for final particles in (a) pp, (b) p-Au and c) Au-Au collision.

The pp and p-Au systems present the similar curved shape on the top of the distribution, except for the high-density region for $y \simeq -0.5$ in the pp system. In contrast, the Au-Au collision system exhibits a flat shape on the top of the distribution. The rapidity range is the same for all three systems.

Analysis for lambda, sigma and kaon particles.

Fig 13 presents the rapidity distribution analysis for lambda(Λ^0), sigma (Σ^+, Σ^0, Σ^-) and kaon (K^0, K^+, K^{*0}, K^{*+}) particles in a) pp, b) p-Au and c) Au-Au collision.

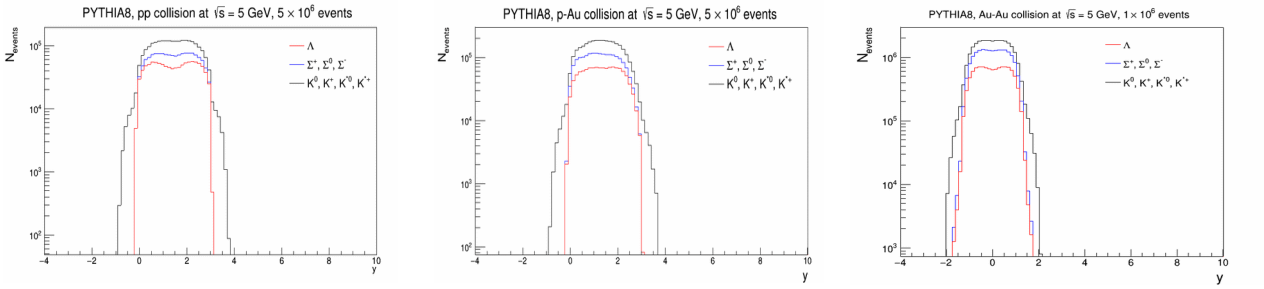

(a) (b) (c)

Fig 13: Rapidity distribution for lambda (red line), sigma (blue line) and kaon (black line) particles in (a) pp, (b) p-Au and (c) Au-Au collision at $\sqrt{s_{NN}}$=5 GeV

We continue to observe not symmetrical distribution, with respect to the origin, in the pp and p-Au collision, which is not present in the Au-Au collision. This is due to the fixed-target collision type considered in the pp and p-Au systems.
The top of the distribution for the three particle types present the same curve in the pp and Au-Au systems.
For all three particles, the rapidity range (-1 $\lesssim$ y $\lesssim$ 4) is the same in both pp and p-Au.
The energy-momentum relation does not for each particle, does not change with system.

Azimuthal angle distribution

The azimuthal angle distribution analysis for final particles and for lambda, sigma and kaon particles individually, in pp, p-Au and Au-Au collision systems is also presented here.

Fig 14 show the analysis for all final particles in a) pp, b) p-Au and c) Au-Au collision at a centre-mass energy of $\sqrt{s_{NN}}$=5 GeV.

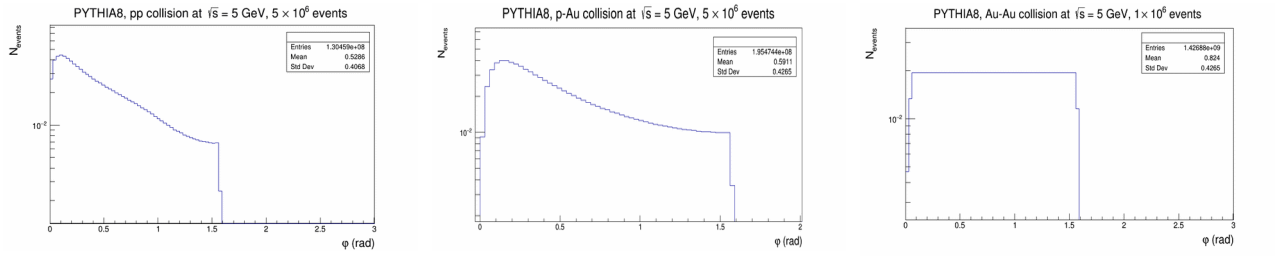

(a) (b) (c)

Fig 14: Azimuthal angle distribution for final particles in a) pp, b)p-Au and c)Au-Au collision at $\sqrt{s_{NN}}$=5GeV

In Fig 14, we observe a similar curved distribution for pp and p-Au collision. In contrast, the Au-Au collision presents an uniform distribution. There are no preferential directions in which the particles of a colliding-beam Au-Au collision are emitted.

Analysis for lambda, sigma and kaon particles.

In Fig 15, we present the azimuthal angle distribution for lambda(Λ^0), sigma (Σ^+, Σ^0, Σ^-) and kaon (K^0, K^+, K^{*0}, K^{*+}) particles in a) pp, b) p-Au and c) Au-Au collision systems at $\sqrt{s_{NN}}$=5GeV. For identified particles, all three colliding systems present a curved shaped, in comparison with the former analysis for the Au-Au system.

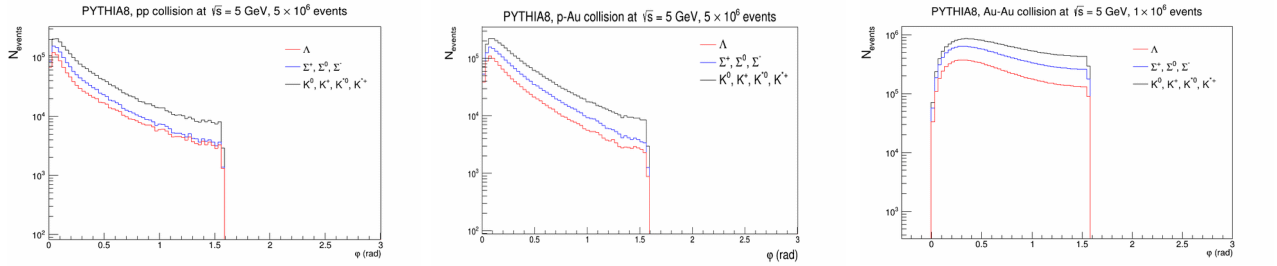

(a) (b) (c)

Fig 15: Azimuthal angle distribution for lambda (red line), sigma (blue line) and kaon (black line) particles in (a) pp, (b) p-Au and (c) Au-Au collision at $\sqrt{s_{NN}}$=5GeV

Conclusions

- We simulated pp, p-Au and Au-Au collision at $\sqrt{s_{NN}}$=5GeV with the PYTHIA8.3 event generator and the Angantyr model.
- The transverse momentum vs longitudinal momentum (p_T vs p_L), transverse momentum vs pseudorapidity (p_T vs η), rapidity and azimuthal angle analysis for all final particles is performed.
- We performed the former analysis for lambda(Λ^0), sigma (Σ^+, Σ^0, Σ^-) and kaon (K^0, K^+, K^{*0}, K^{*+}) particles individually to study strange particle production.
- Results on the "p_T vs p_L" and "p_T vs η" general, and particular for lambda, sigma and kaon particles, analysis agree with expectations.
- The results for the azimuthal angle distribution for all final particles, in the Au-Au collision, could be attributable to a defect in the simulation code.

Reference

[1] STAR Collaboration, "STAR detector overview", Nuclear Instruments and Methods in Physics Research Section A: Accelerators, Spectrometers, Detectors and Associated Equipment, Volume 499, Issues 2–3, 2003, Pages 624-632, ISSN 0168-9002. DOI: 10.1016/S0168-9002(02)01960-5

[2] Sorin A.S, Teryaev O. V, Meshkov I. N, Trubnikov G. V, G. G. Khodzhibagiyan, Kovalenko A.D, Butenko A. V, Sidorin A. O, Syresin E. M, Golovatyuk V. M, Kapishin M. N, Tsenov R, Syresin E. M, Dolbilov A.V, Yu. K. Potrebenikov, Agapov N. N, Dudarev, A.V, Semin N. V, Trubnikov B. A, *Technical project of the object "NICA Complex"*, 2018. https://nica.jinr.ru/documents/TDR_spec_Fin0_for_site_eng.pdf

[3] Nuclotron-based Ion Collider fAcility (NICA) https://nica.jinr.ru/complex.php

[4] Adam Kisiel, The NICA Complex and the MPD experiment at JINR: status and physics potential. EPJ Web Conf. 259 09002 (2022) DOI: 10.1051/epjconf/202225909002

[5] D. Blashke et. al. Exploring strongly interacting matter at high densities - NICA White Paper. EPJ A. V 52, N8, 2016. 267 p.
http://theor0.jinr.ru/twiki/pub/NICA/WebHome/WhitePaper_10.01.pdf

[6] Spin Physics Detector (SPD) project https://spd.jinr.ru/

[7] Baryonic Matter at Nuclotron (BM@N) https://bmn.jinr.ru/

[8] Multi-Purpose Detector (MPD) https://mpd.jinr.ru/

[9] S. Porteboeuf, T. Pierog, K. Werner, Producing Hard Processes Regarding the Complete Event: The EPOS Event Generator (2010). DOI: 10.48550/arXiv.1006.2967

[10] S. A. Bass, M. Belkacem, M. Bleicher, M. Brandstetter, L. Bravina, C. Ernst, L. Gerland, M. Hofmann, S. Hofmann, J. Konopka, G. Mao, L. Neise, S. Soff, C. Spieles, H. Weber, L. A. Winckelmann, H. Stöcker, W. Greiner, Ch. Hartnack, J. Aichelin, N. Amelin, "Microscopic Models for Ultrarelativistic Heavy Ion Collisions", Progress in Particle and Nuclear Physics, V 41 (1998). DOI: 10.1016/s0146-6410(98)00058-1

[11] Simulating Many Accelerated Strongly-interacting Hadrons SMASH https://smash-transport.github.io

[12] The STAR Experiment physics results summaries
https://www.star.bnl.gov/central/physics/results/

[13] B. Andersson, G. Gustafson and B. Nilsson-Almqvist, "A model for low-pT hadronic reactions with generalizations to hadron-nucleus and nucleus-nucleus collisions", Nucl. Phys B 281: 289-309 (1987) DOI:10.1016/0550-3213(87)90257-4

[14] STAR Collaboration, "Flow and interferometry results from Au+Au collisions at $\sqrt{s_{NN}}=4.5\,GeV$, Physical Review C 103: 2469-9993 (2021). DOI: 10.1103/PhysRevC.103.034908

[15] STAR Collaboration, "Probing Strangeness Canonical Ensemble with K^-, $\phi(1020)$ and Ξ^- production in Au+Au Collisions at $\sqrt{s_{NN}}=3\,GeV$", Physics Letters B 831:0370-2693 (2021) DOI: 10.1016/j.physletb.2022.137152

[16] STAR Collaboration, "Production of Protons and Light Nuclei in Au+Au Collisions at $\sqrt{s_{NN}}=3\,GeV$ with the STAR Detector" (2023) arXiv: https://arxiv.org/abs/2311.11020